COLLAPSE MECHANISM ANALYSIS OF HISTORIC MASONRY STRUCTURES SUBJECTED TO LATERAL LOADS: A COMPARISON BETWEEN CONTINUOUS AND DISCRETE MODELS

Marialaura Malena[1], Francesco Portioli[2 *], Raffaele Gagliardo[2],
Giovanni Tomaselli[1], Lucrezia Cascini[2] and Gianmarco de Felice[1]

[1]*Department of Engineering, University of Roma Tre, Italy.*
[2]*Department of Structures for Engineering and Architecture, University of Naples "Federico II", Italy*

ABSTRACT

The aim of this paper is to show to what extent a simple constitutive model can adequately describe the collapse mechanisms of historic masonry structures under horizontal seismic loads. Referring to block masonry, the paper presents the formulation and the numerical implementation of a constitutive relationship for modeling masonry structures regarded at a macroscopic scale as homogenized anisotropic continuum. The macroscopic model is shown to retain memory of the mechanical characteristics of the joints and of the shape of the blocks. The overall mechanical properties display anisotropy and singularities in the yield surface, arising from the discrete nature of the block structure and the geometrical arrangement of the units. The model is formulated in the framework of multi-surface plasticity. It is implemented in a FE code by means of a minimization algorithm directly derived from the Haar-Karman principle.

A sensitivity analysis to mechanical and geometrical parameters was carried out to show the influence on the predicted response of small-scale wall components from the literature. The model is then used for the analysis of a numerical case study which is representative of a masonry church subjected to horizontal seismic action.

The result of the model will be compared with those obtained by a rigid block model (RBM) of the same small-scale masonry prototypes and of the church building. In the paper, the results of the two models are discussed and analyzed in the way to highlight the weakness and the potentiality of the two different approaches.

Keywords: Historic Masonry Structures; FE Path Following Analysis; Rigid Block Limit Analysis; In-plane and out-of-plane failure modes; Collapse load factors.

1. INTRODUCTION

The response of historic masonry structures under seismic events is usually affected by local failure mechanisms which typically involve both in-plane and out-of-plane collapse modes (Fig. 1). The assessment of the seismic capacity related to these failure mechanisms can be carried out using different analysis types and modelling approaches [1-6].

A simple method to assess the seismic capacity is linear kinematic analysis [3, 4], which is essentially based on the prediction of the likely failure modes of the construction and the evaluation of the magnitude of lateral loads that activate the collapse modes. Those are usually expressed as a factor of vertical dead loads (i.e. self-weight and floor loads) by means of the collapse load multiplier.

Considering the uncertainties that typically affect the structural knowledge of these historic structures, numerical models suitable for linear kinematic analysis of entire constructions should be as simple as possible and should be based on few mechanical parameters. The essential features to be considered are the ability to capture the failure in traction and the possibility to include the anisotropic behavior of masonry, at least in terms of failure conditions. In addition, the capability to reproduce the damage patterns under different boundary and loading conditions (in-plane and out-of-plane) should be provided as well.

Similar modelling approaches were adopted in recent national standards and commentaries comprising linear kinematic analysis (also addressed as force-based assessment method) for the safety assessment of local failure mechanism [7, 8]. According to these standards, a simple modelling approach is to discretize historic structures into assemblages of infinitely resistant bodies interacting at no-tension, frictional contact interfaces.
When the failure mechanism is self-evident and can be easily schematized into single or few blocks forming a single degree of freedom kinematic chain, simple analytical formulations based on the principle of virtual works can be derived for the calculation of the corresponding value of the collapse load multiplier.
For complex and three-dimensional structures, crucial to the application of the linear kinematic analysis is the use of appropriate modelling approaches for the calculation of the lower collapse load multiplier and the corresponding failure mechanism.

In this framework, a variety of modelling approaches was proposed in past decades [9]. Among those, homogenized continuous finite element models and discrete rigid block models represent two different alternatives that are commonly used for the prediction of local failure mechanism in historic masonry structures [9-31].

The use of homogenized FE models or rigid block models for collapse mechanism analysis involves different strengths and weaknesses, which are mainly concerned with the ability to simulate the highly nonlinear and anisotropic behavior of masonry for in-plane and out-of-plane loads, not only at the scale of single structural elements but also in case of entire monuments.

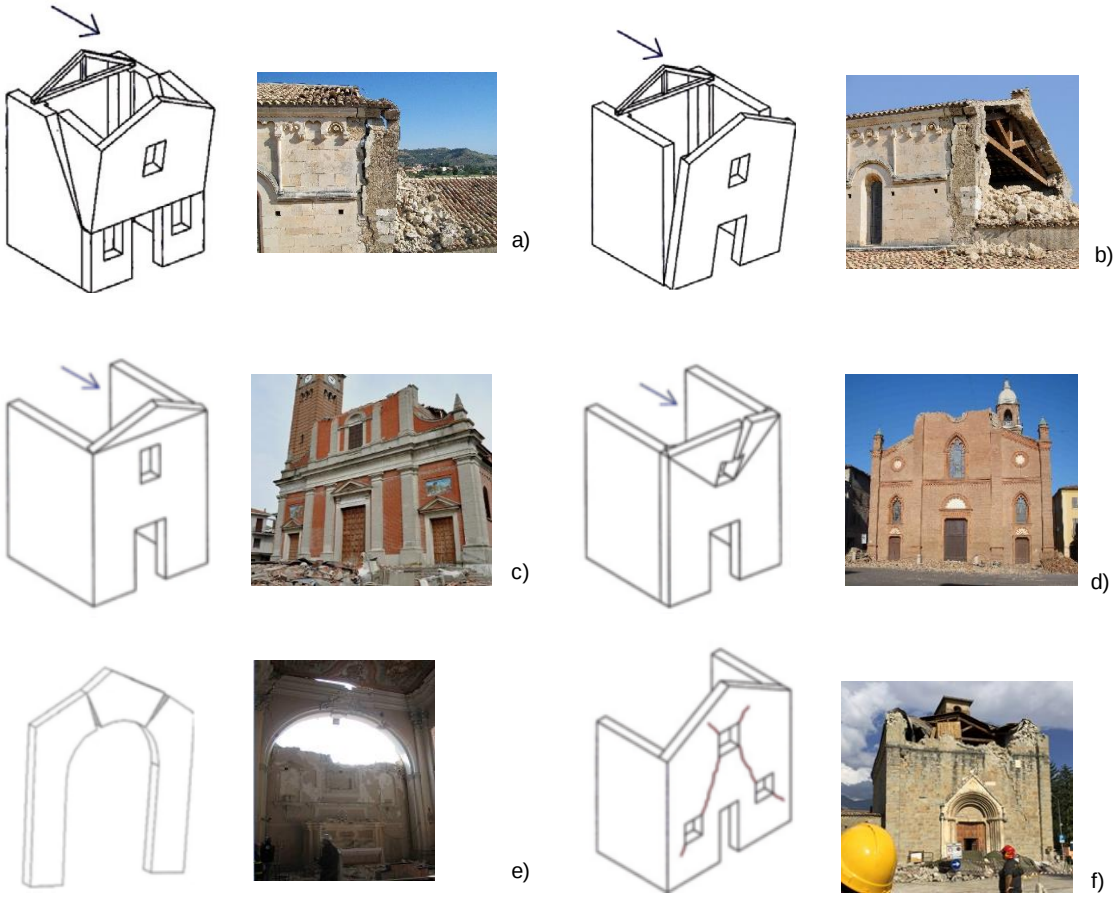

FIGURE 1. Examples of failure mechanisms from damage surveys after earthquake [35].

In this perspective, the aim of this study was to compare the results obtained from a continuous finite element and a discrete rigid block model, in order to evaluate potentialities and limitations of the selected modelling approaches when applied to the analysis of collapse mechanisms of the same cases study.

The first model adopted is a discrete element model for three-dimensional limit analysis, which is made of rigid blocks interacting at no-tension, frictional contact interfaces [33].
The model used for contact interaction is a point-based contact model. This model represents a simple alternative to the classic surface contact model (with static variables associated to stress resultants acting at a single point, i.e. the center of contact interface) which strongly simplifies the formulation of the mathematical programming problems associated to limit equilibrium analysis of collapse mechanisms [33].

When a point-based contact model is used, the corresponding limit analysis problems can be cast as simple second order cone problems, for which very efficient solution algorithm exists. Comparisons against alternative rigid block formulations which stem from the linear complementarity problems associated to the system of equilibrium, failure and compatibility conditions showed that solutions can be obtained with shorter CPU time, by up to two order of magnitude [32].

Another key feature of the adopted rigid block model is the ability to take into account non-associative sliding behaviour by means of a simple heuristic iterative solution procedure firstly presented by Gilbert and his co-workers for 2D assemblages using a different contact model, namely a surface contact model [43].

However, applications of the proposed model to entire historic masonry buildings still represent a challenging task, both for computational and geometric modelling issues. Considering the large number of blocks which are comprised in these cases, alternative solution procedures of the underlying optimization problem could be used to save additional CPU time. Other issues concern the development of efficient tools and algorithms for the generation of spatial rigid block models involving complex bond patterns, which might facilitate users' application and implementation of the proposed formulation [44].

The second model considered is a nonlinear three-dimensional finite element model [20-22]. The masonry wall is represented as an elasto-plastic homogenized Love-Kirchhoff plate with an associated flow-rule. The model was formulated in the framework of multi-surface plasticity and it was implemented in a FE code by means of a minimization algorithm directly derived from the Haar-Karman principle.

The numerical analyses carried out by the above-mentioned model are path following analyses able to provide the capacity curves derived from pushover analyses and expressing the variation of the collapse load multiplier as a function of a control point displacement.

The rigid block and the finite element model were validated in previous studies against a set of numerical benchmark problems and small-scale experimental case studies subjected to in-plane and out-of-plane failure modes [22,30,32,34-36]. It has been shown that the failure mechanisms and collapse load multipliers predicted are very similar to those considered and that accurate solutions are obtained with reduced computational costs.

In this work, a comparison of those models is presented to show sensitivity to algorithm and mechanical parameters as well as to block size ratio and in order to evaluate differences and computational efficiency when the collapse mechanism analysis of an entire full-scale monumental building is carried out.

In the case of the rigid block model, a different numerical procedure was also implemented in order to evaluate the convergence sensitivity to starting conditions and to explore the possibility of improving the computational efficiency of the iterative solution algorithm used to take into account non-associative sliding.

The case study considered for collapse mechanism analysis is a masonry church subjected to horizontal loads induced by seismic actions. Comparisons between the two modelling approaches considered were carried out in terms of failure mechanisms and deformed configurations, as well as in terms of lateral loads promoting the collapse. The aim of this comparison was also to show the ability of the adopted continuous model in capturing the response of a masonry building where different bond patterns are used for structural elements.

The paper is organized as follows. The relationships governing the behavior of the rigid block model and the formulation of the limit analysis problem are discussed in Section 2. The formulation of the homogenized anisotropic constitutive model adopted for FEA is presented in Section 3. Results of the sensitivity analysis to mechanical and algorithm parameters are presented in Section 4. The case study of the masonry church considered for application is described in Section 5. In Section 6 the results obtained from FEA and RBLA are presented. Comparisons, potentialities and drawbacks of the modelling approaches adopted are also discussed in this Section.

2. THE RIGID BLOCK MODEL FOR LIMIT ANALYSIS

In the adopted rigid block model, historic masonry structures are represented as assemblages of rigid blocks *i* interacting at the interfaces *j* (Fig. 2a, 2b). A no-tension, frictional behaviour with infinite compressive strength is assumed at contact interfaces [32].

The calculation of the load factor α expressing the magnitude of lateral loads promoting the collapse is obtained from the solution of the static (i.e. lower bound) formulation of the limit analysis problem. The limit analysis problem is formulated in terms of second order cone programming, as follows:

$$\begin{aligned} \max \quad & \alpha \\ \text{s.t.} \quad & \boldsymbol{A}\,\boldsymbol{c} = \boldsymbol{f_D} + \alpha \boldsymbol{f_L} \\ & \boldsymbol{c} \in C \end{aligned} \tag{1}$$

In the above optimization problem, the first constraint represents equilibrium conditions between internal static variables associated to contact interactions and external loads. The static variables are the internal forces acting at contact points *k*, located at the vertexes of each interface. Those are collected in vector $\boldsymbol{c}$ and include the shear force components t_{1k} and t_{2k} and

the normal force n_k at each contact point, acting along the tangent and normal direction to contact interface. External loads applied to the centroid of rigid block *i* are expressed as the sum of dead loads $\boldsymbol{f_D}$ and live loads $\boldsymbol{f_L}$ multiplied by the collapse load factor α. $\boldsymbol{A}$ is the ($6b \times 3c$) equilibrium matrix, being *b* the number of blocks and *c* the number of contact points.

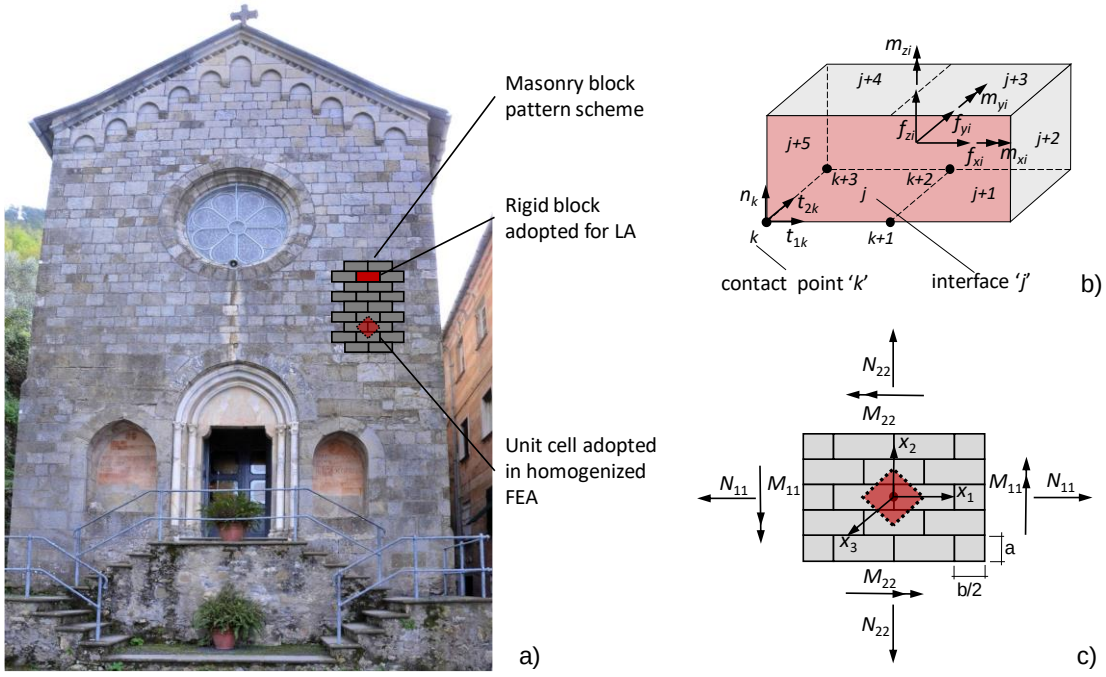

FIGURE 2. a) Example of a historic church made of stone blocks (S. Nicolò di Capodimonte, Camogli, Italy) and schematization of masonry pattern used in rigid block and finite element modelling; b) rigid block *i* with external loads acting at the centroid, interfaces *j* and contact points *k* with internal forces; c) scheme of unit cell and internal forces in the homogenized finite element model.

The second constraint represents the Coulomb failure condition described by the convex cones:

$$\boldsymbol{C} = \left\{ \mu\, n_k \geq \sqrt{t_{1k}^2 + t_{2k}^2}\,,\; n_k \geq 0 \right\}, \tag{2}$$

being μ the friction coefficient.

The solution of the static problem (1) involves associative behaviour (i.e. normality rule) when sliding occurs at a contact point, with normal displacement rates accompanying tangential displacement rates (i.e. dilatancy). It is worth noting that the assumption of associative behaviour might involve collapse load multipliers which represent upper bounds on the load factors corresponding to non-associative friction model, i.e. to zero-dilatancy sliding behaviour. To take into account non-associative (zero dilatancy) behaviour for sliding failure, for which a lower and hence safe value of the collapse load multiplier can be obtained, a simple iterative solution procedure is implemented. Iterations are carried out solving a series of mathematical programming problems of type (1) and using a fictitious failure condition rather than the

Coulomb friction cone (Fig. 3). The fictitious failure condition is characterized by a friction angle equal to zero and by a fictitious cohesion (updated at each iteration), so that the associated normality rule involves a zero-dilatancy behaviour.

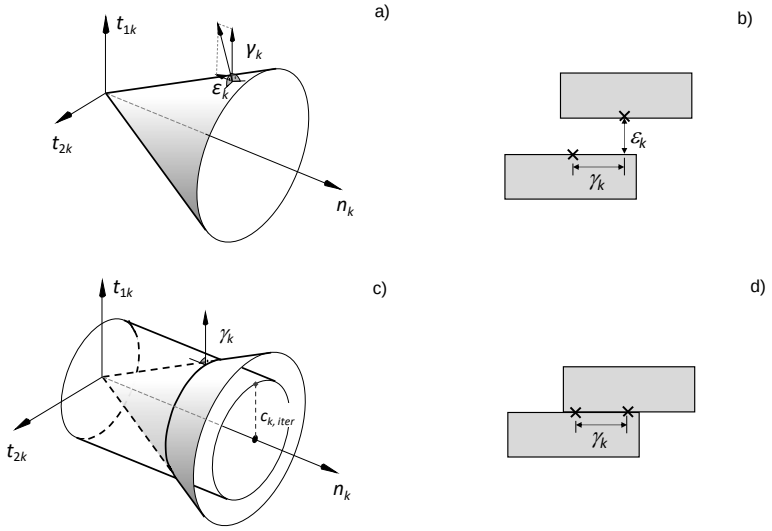

FIGURE 3. a) Failure surface for pure shear, also showing associative displacement rates; b) sliding failure mode with dilatancy (associative behaviour); c) Fictitious failure surfaces used in the iterative solution procedure to restore zero dilatancy; d) sliding failure mode with zero dilatancy (non-associative behaviour) [30].

The fictitious cohesion is calculated as follows:

$$c_{k,\text{iter}+1} = \left(\beta n_{k,\text{iter}} + (1-\beta) n_{k,\text{iter}-1}\right)(1+\xi)\mu + c_k^0, \tag{3}$$

where: β is an algorithm parameter used to calculate normal forces $n_{k,\text{iter}+1}$ at iteration no. *iter+1* on the basis of normal forces computed at previous iterations and c_k^0 is a small cohesion value which is introduced to overcome numerical convergence problems when the normal force at a contact point tends to zero. The parameter ξ governs the angle of friction of the fictitious failure surface.

In the present study, starting values of normal forces corresponding to a uniform distribution of normal forces n_0 are also used as an alternative to the normal force distribution $n_{assoc.}$ corresponding to the associative solution, as it was in the iterative solution procedure presented in [32]. The uniform normal force distribution was used to check sensitivity of results to starting conditions and also to explore the possibility to save CPU time in case of large scale problems, as illustrated in Section 6, considering that in this case the calculation of the associative solution is not necessary to start the iterative solution procedure.

The implemented procedure to take into account non-associative behaviour is summarized in the following algorithm:

(1) Initialize the iterative solution procedure: Set iteration number *iter*=0; $n_{k,iter} = n_0$ and $n_{k,iter-1} = 0$ at each contact point;

(2) Start the iterative solution procedure. Set *iter*=*iter*+1, calculate starting values of fictitious cohesion using Eq (3) and define failure conditions (2);

(3) Set up and solve SOCP problem (1) and obtain α_{iter} and a new distribution of normal forces $n_{k,iter}$

(4) If $\frac{\alpha_{iter}-\alpha_{iter-1}}{\alpha_{iter}} \leq tol$, then exit, else repeat from step (2)

For the numerical simulations presented in this study, the converge tolerance *tol* was set equal to 1e-3 and the cohesion c_k^0 was equal to 1e-4 n_{max}, being n_{max} the maximum value of normal force calculated at a given iteration. The algorithm parameters β and ξ were set equal to 0.6 and in the range 0 to 1e-2, respectively, according to [30].

The primal-dual interior-point solver MOSEK 8.0.0.81 was used to solve the mathematical programming problems associated to limit equilibrium analysis.

3. FORMULATION OF THE HOMOGENIZED CONSTITUTIVE MODEL FOR FEA

The finite element model [20-22] represents the masonry wall as an elasto-plastic homogenized Love-Kirchhoff plate, with an associated flow-rule. It is formulated in the framework of infinitesimal multi-surface rate-independent plasticity.

According to elasto-plasticity theory, the stress-strain relationship of the macroscopic homogenized plate, can be written as:

$$\mathbf{t} = \mathbf{C}:(\boldsymbol{\varepsilon} - \boldsymbol{\varepsilon}^{p}) \tag{4}$$

where the vector **t** collects the macroscopic in plane (membrane) **N** = $N_{\alpha\beta}$ and out of plane (bending) **M** = $M_{\alpha\beta}$ stress field, while the vector **ε** collects the corresponding total macroscopic in plane **E** = $E_{\alpha\beta}$ and out of plane χ = $\chi_{\alpha\beta}$ strain rate field, for α, β= 1..2. The vector $\boldsymbol{\varepsilon}^{p}$ collects the plastic strain field and **C** is the orthotropic elastic stiffness tensor of the homogenized masonry wall defined as described in [22].

In order to represent masonry wall as an elasto-plastic macroscopic continuum, the elastic domain associated with it has to be defined. It was assumed to coincide with the macroscopic strength domain defined in [20-21], derived by a homogenization procedure applied to a thin and periodic heterogeneous plate, made of 3D infinitely resistant blocks connected by Mohr-Coulomb interfaces. The macroscopic elastic domain assumes the following form:

$$E_t = \left\{\mathbf{t} := (\mathbf{N},\mathbf{M}) \middle| f^i(\mathbf{N},\mathbf{M}) := \mathbf{N}:\mathbf{E} + \mathbf{M}:\boldsymbol{\chi} - c^i \leq 0 \ \forall \ i \in [1,..,m]\right\} \tag{5}$$

where $f^i(\mathbf{t})$ are m independent planes intersecting in a non-smooth way. According to [20-21], it is possible to write the $m=8$ planes, in terms of stress components in the Ox_1x_2 plane as follows:

$$f^{1-2} := \mu_b N_{11} + tg(\phi)N_{22} \pm (1 + tg(\phi)\mu_b)N_{12} - h\left(c + \frac{c\mu_b}{tg(\phi)}\right) \leq 0$$

$$f^{3-4} := N_{22} \pm \frac{1}{tg(\phi)}N_{12} - \frac{hc}{tg(\phi)} \leq 0$$

$$f^{5-6} := N_{22} \pm \frac{2}{h}M_{22} - \frac{hc}{tg(\phi)} \leq 0 \qquad (6)$$

$$f^{7-8} := (p+q)N_{22} \pm \frac{2}{h}M_{11} - \frac{2}{h}(q-p)M_{22} - \frac{h(p+q)c}{tg(\phi)} \leq 0$$

with:

$$p = \frac{tg(\phi)}{\mu_b}\frac{b}{4h} \qquad q = \frac{tg(\phi)}{\mu_b}\sqrt{1 + \left(\frac{b}{4h}\right)^2} \qquad (7)$$

The elastic domain depends explicitly on the cohesion c and on the friction angle ϕ of the joints, on the aspect ratio $\mu_b = \frac{2a}{b}$ of the blocks, being a the height and b the width of the blocks, and on the thickness h of the plate (Fig. 2a, 2c). It is anisotropic as a consequence of the arrangement of the blocks within the assembly and it is unbounded in the direction of compression [22].

Finally, the evolution of plastic strain field ε_p in Eq. (3), is controlled by the associated flow rule expressed as proposed by Koiter [39]:

$$\dot{\varepsilon}^p := \sum_{i=1}^{m} \dot{\gamma}^i \frac{\partial f^i(\mathbf{t})}{\partial \mathbf{t}} \qquad (8)$$

where $\dot{\gamma}_i$ are the m plastic multipliers, subject to the Kuhn-Tucker conditions for $i \in [1..m]$:

$$\dot{\gamma}^i \geq 0; \quad f^i(\mathbf{t}) \leq 0; \quad \dot{\gamma}^i f^i(\mathbf{t}) \equiv 0 \qquad (9)$$

and to the consistency condition $\dot{\gamma}^i \dot{f}^i(\mathbf{t}) \equiv 0$.

The assumption of associated flow rule may be not completely satisfactory in the case of block structures, since the blocks may slide with no dilation, giving rise to a non-associated flow rule at the macroscopic scale. If this assumption, on the structural viewpoint, may lead to an overestimate of the ultimate load as clearly pointed out in [40], at the same time, it allows to handle the numerical formulation by means of a convenient minimization procedure [22,41-42].

The solution of the system of equations, obtained by integrating Eqs.(4) and (8) in terms of finite increments [35], according to the Haar Karman's principle, coincides with the following minimization problem:

$$\begin{cases} \text{minimize}: \Pi_{HK}[\Delta\mathbf{t}_{n+1}] = \frac{1}{2}\left(\Delta\mathbf{t}_{n+1} : \mathbf{C}^{-1} : \Delta\mathbf{t}_{n+1}\right) \\ \text{subject to}: \quad f^i(\Delta\mathbf{t}_{n+1}) \geq 0 \quad \text{for } i \in [1,..,m] \end{cases} \qquad (10)$$

where the subscript *n+1* denotes the new solutions $\{\mathbf{t}_{n+1}, \boldsymbol{\varepsilon}^{p}_{n+1}\}$ to be determined with respect to the known state $\{\mathbf{t}_{n}, \boldsymbol{\varepsilon}^{p}_{n}\}$ and the assigned total strain $\boldsymbol{\varepsilon}_{n+1}$, while $\Delta\mathbf{t}_{n+1} \coloneqq \mathbf{t} - \mathbf{t}_{\mathrm{E}}$, being $\mathbf{t}_{\mathrm{E}}$ the elastic predictor related to the total strain increment through the elastic tensor **C**.

4. SENSITIVITY ANALYSIS ON SMALL SCALE WALL COMPONENTS

Numerical simulations based on two tilting tests carried out at the University of Pavia [45] on 1:5 scale dry-stone masonry prototypes were performed to compare the outcomes deriving from the two different approaches. A sensitivity analysis to friction coefficient, block size ratio, RBM starting conditions and FE mesh size was also carried out to evaluate the effects on the predicted response.

4.1. Comparisons against experimental tests

The two tests were selected to compare the predicted response for both the in-plane and the out of plane behaviour.

The first prototype analysed is the S22, made of a main wall and three partition walls with openings. The main wall was 21 bricks high and 14 bricks wide, while the partition walls were 21 bricks high and 10 bricks wide with one opening each, 15 bricks high and 2 bricks wide.

The second numerical simulation deals with the S5 prototype, made of a main wall and two partition walls. The main wall is 21 bricks high and 8 bricks wide, while the partition walls are 21 bricks high and 4 bricks wide.

Masonry prototypes were made of blocks whose dimensions are equal to 30x80x40 mm^3, the unit weight of the masonry is 28.6 $\frac{KN}{m^3}$, while the friction coefficient μ was assumed equal to 0.7. All the mechanical parameters needed for the finite element simulations are summarized in Table 1, where t is the thickness of the joints, E_b, ν_b and E_m, ν_m are the Young modulus and the Poisson ratio for block and mortar joints, respectively. These last parameters being required for the definition of the elastic tensor **C** [23, 30]. Due to the absence of mortar, the shear strength along the dry joints was due to pure friction with cohesion c = 0.

TABLE 1. Mechanical parameters for FE model.

a [mm]	b [mm]	h [mm]	E_b [GPa]	E_m [GPa]	t [mm]	ν_b	ν_m
30	80	40	3.18	0.303	1	0.23	0.3

Numerical simulations of the tilting tests were performed considering that blocks were subject to self-weight loading and to varying horizontal loads associated to blocks self-weight and tilt angle. In the case of the rigid block model, this loading condition was simply reproduced

considering horizontal live loads expressed as a function of the load factor α and block self-weight.

In the case of the FE model, the loads were applied in two steps, that is applying the self-weight to masonry walls at first and, in sequence, horizontal forces proportional to the self-weight. The load factor, defined as the ratio between the horizontal and the vertical components of the body forces, was increased from 0 up to α_c, corresponding to the collapse of the wall.

In Figure 4 the results obtained for the S22 experimental test are represented in terms of plastic strains at collapse for the FE model. The failure modes obtained from the RB model for the associative and non-associative solution are also shown for comparison.

The comparison of associative failure modes shows a good agreement between predicted collapse mechanisms. At collapse, the main feature of the crack pattern was the strong concentration of in plane joint opening in the partition walls close to the door, for both the models. In the case of the RB model, different crack patterns can be noted in the spandrels above the openings for the non-associative solution, which are very similar to those observed experimentally.

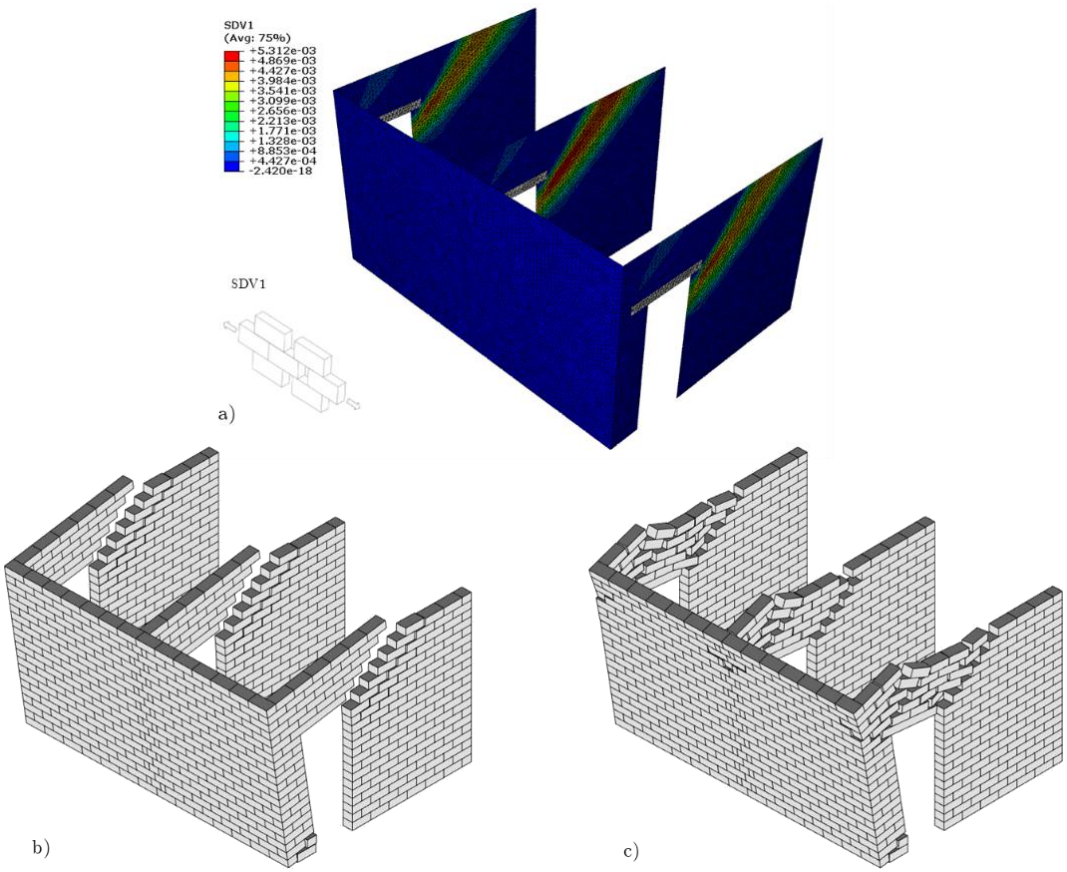

FIGURE 4. Test S22 (α_{exp}=0.197) [45]: a) plastic strain distribution at collapse for FE model (α_c=0.182); b) associative and c) non-associative failure mechanism for RB model (α_{assoc}=0.208, $\alpha_{non\text{-}assoc}$=0.186).

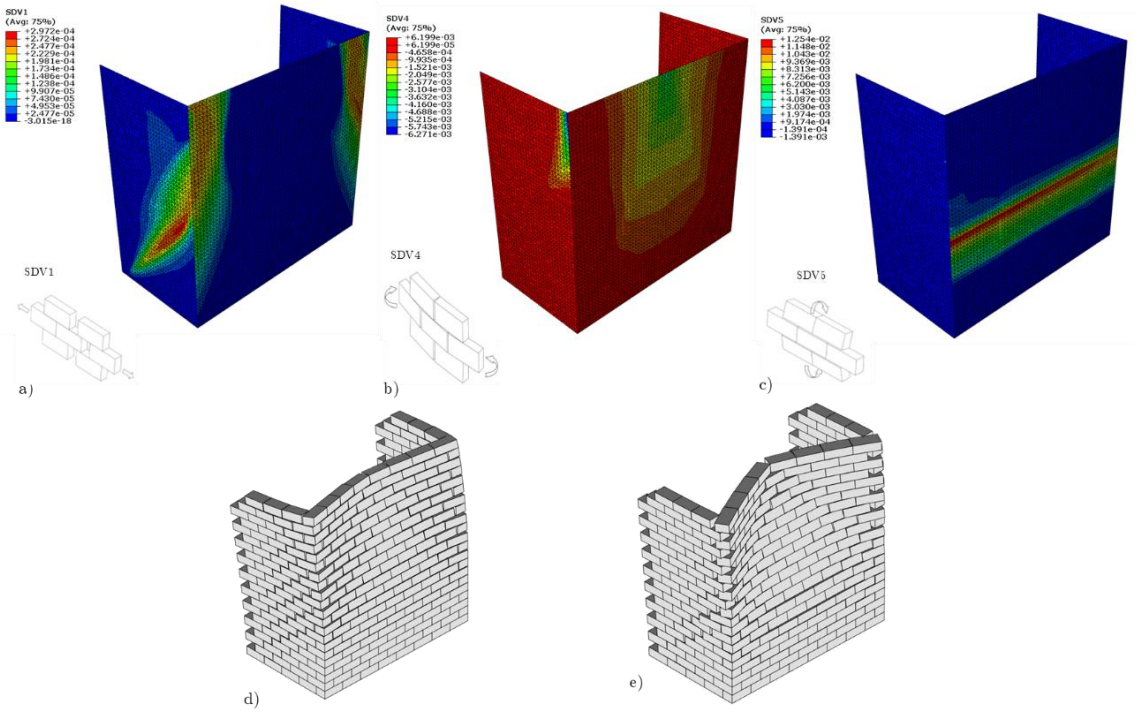

FIGURE 5. Test S5 (α_{exp}=0.349) [45]: a)-c) plastic strain distribution at collapse for FE model (α_c=0.298); d) associative and e) non-associative failure mechanism for the RB model (α_{assoc}=0.448, $\alpha_{non\text{-}assoc}$=0.380).

The failure mechanisms derived from the simulation of the S5 experimental test with the RBM and the FE model are presented in Figure 5. The plastic strain distribution corresponding to the opening of the bed and the head joints are reported for the FE model.

The crack pattern at the collapse was characterized mainly by the bending opening of the head joints in the central portion of the main wall interested by out of plane overturning and by the in plane opening of the head joints in the partition walls.

About the comparison between experimental test and predicted collapse load multipliers, in the case of the finite element model the difference was equal to -8.2% and -14.9% for test S22 and S5, respectively. In the case of numerical simulations by the rigid block model, the discrepancy in terms of load factor between experimental test and numerical model was equal to +5.5% and -5.6% for test S22 and +28.4% and +8.9% for test S5, for the associative and non-associative behaviour, respectively. While the numerical outcomes for the test S22 match quite well with the observed behaviour, the results for the S5 are affected by a larger difference. A remarkable difference can be also noted between the associative FE and the RB solutions in the case of the test S5. This difference can be mainly ascribed to the simple contact model adopted in the case of the rigid block model, which produces an overestimation of the load factor when torsion behaviour is involved [46, 47].

4.2. Sensitivity analysis to friction coefficient and block size ratio

Sensitivity analyses to friction coefficient and to the block size ratio were carried out with the FE and RB model. The results obtained in terms of load factor in the case of S22 are presented in Fig. 6a.

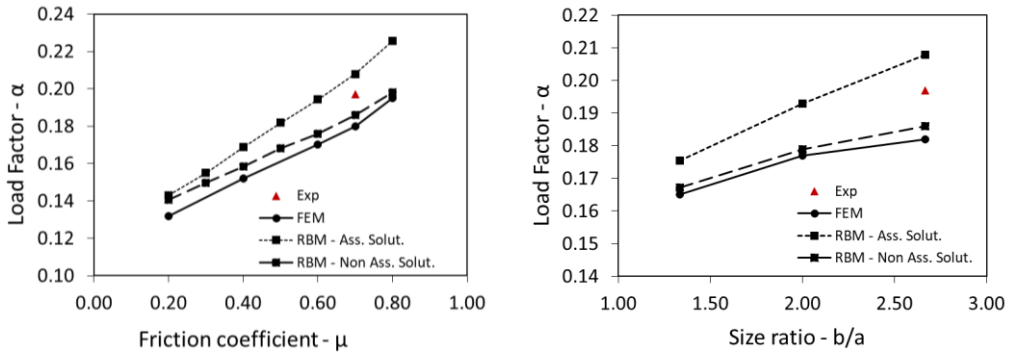

FIGURE 6. Test S22: a) sensitivity analyses to the friction coefficient and b) to the block size ratio.

As expected, lower values of the load factor are obtained when reducing the friction coefficient, for both the models. In terms of crack pattern at the collapse, the reduction of the friction coefficient caused the development of a wider area involved in the opening of the joints, as shown in Fig. 7, where the outcomes for $\mu = 0.4$ are reported.

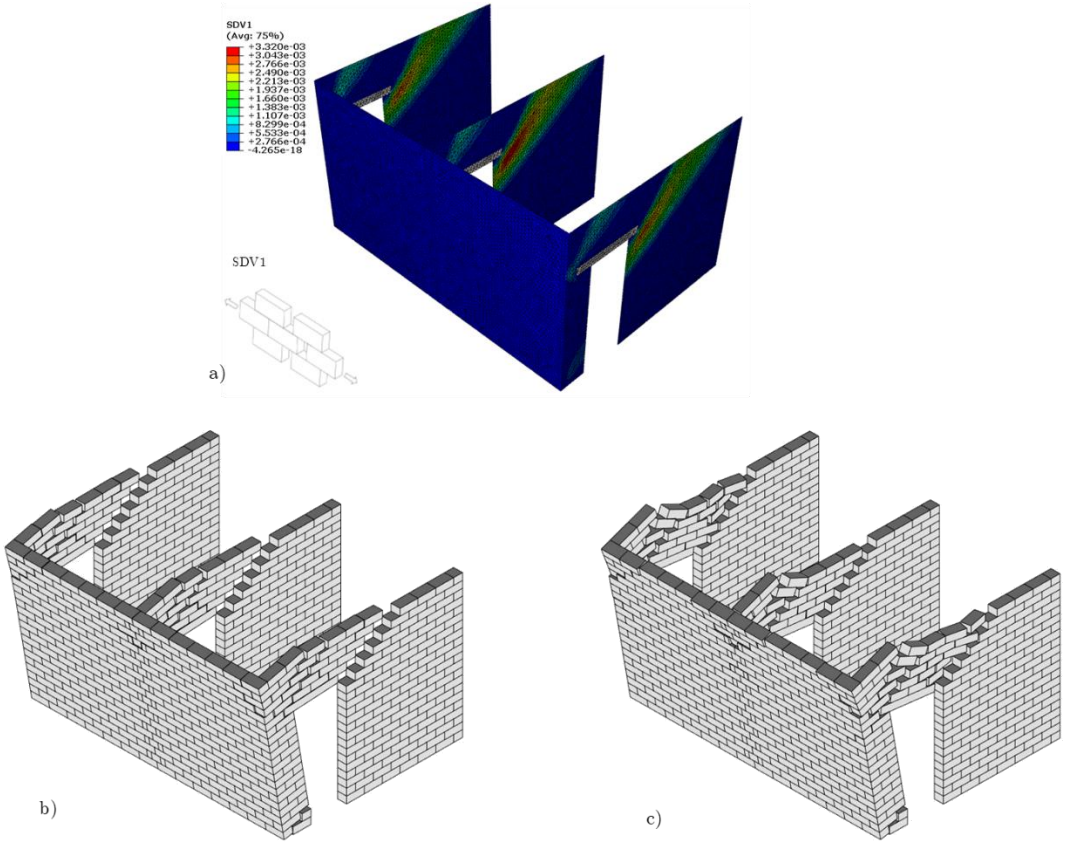

FIGURE 7. Test S22: sensitivity analyses to the friction coefficient ($\mu = 0.4$ in the Figure). a) Plastic strain distribution for FE model; b) associative and c) non-associative failure modes predicted with the RB model.

When varying the size ratio *b/a* and more in detail fixing the height *a* = 30mm and reducing the width *b*, lower values of the load factor are obtained (Fig. 6b). In Fig.8 the results in terms of crack pattern at the collapse are reported for *b*=40mm, where a wider area involved into the in-plane joints opening can be noted in the case of the FE model.

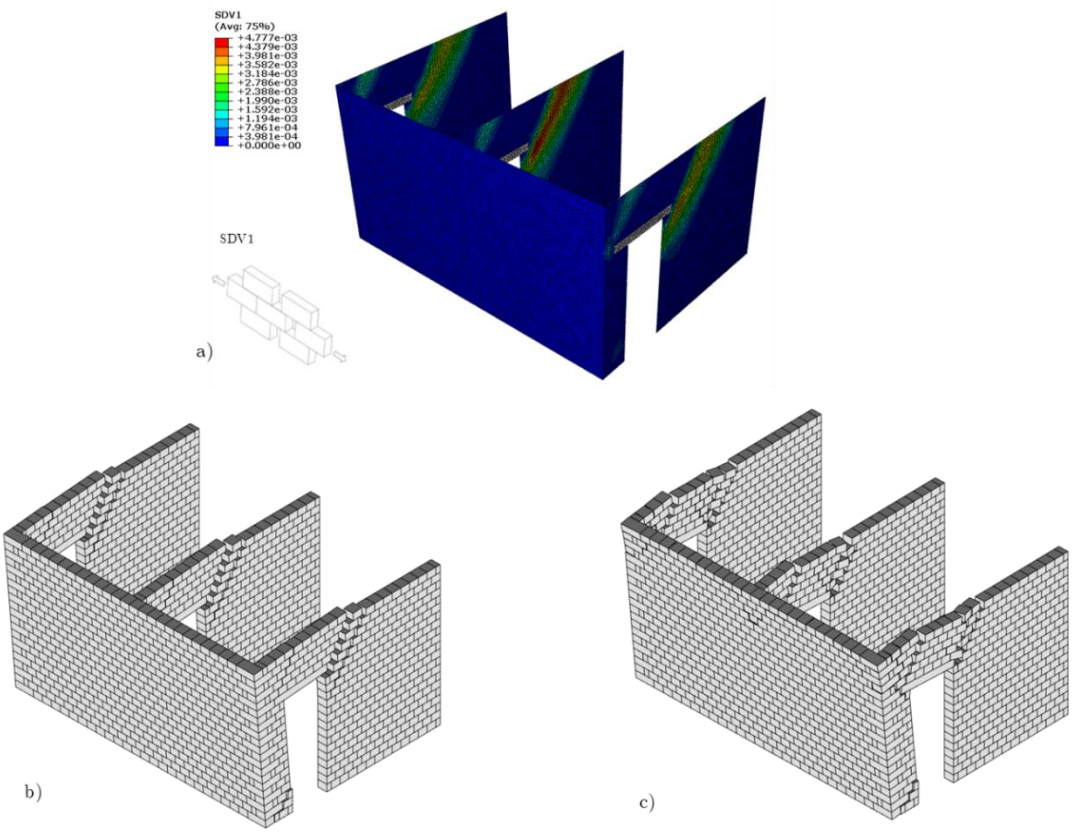

FIGURE 8. Test S22: sensitivity analyses to the size ratio (b=40 mm in the Figure). a) Plastic strain distribution for FE model; b) associative and c) non-associative failure modes predicted with the RB model.

The results of sensitivity analyses carried out on test S5 are shown in Fig.9. Also in this case, lower values of the load factor are obtained when reducing the friction coefficient, for both the models. In terms of crack pattern at the collapse, the reduction of the friction coefficient caused an overturning of the main wall less localized in its upper part, as highlighted in Fig. 10 where the results for $\mu = 0.4$ are reported.

Also in this case, lower values of the load factor are obtained when the size ratio *b/a* is reduced (Fig. 9b). In Figure 11, the results in terms of crack pattern at the collapse for the case *b*=40mm are shown for both the models. The reduction of the size ratio does not affect the portion of the main wall involved in the overturning but increases the intensity of the joints opening.

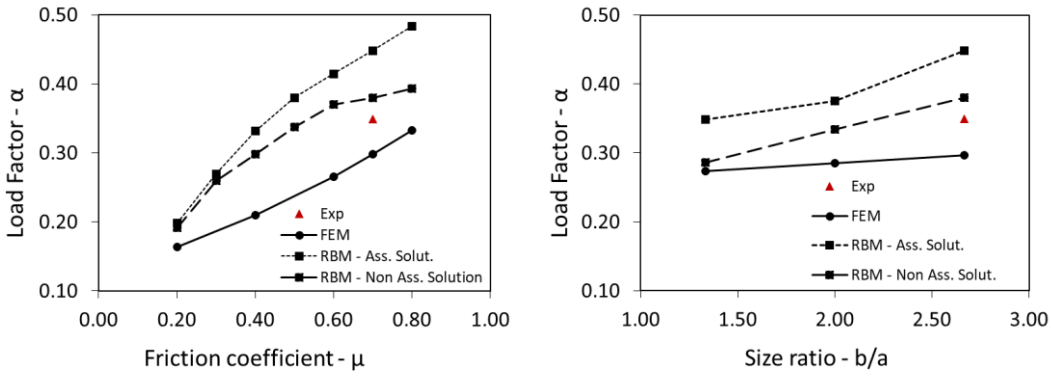

FIGURE 9. Test S5: a) sensitivity analyses to the friction coefficient and b) to the block size ratio.

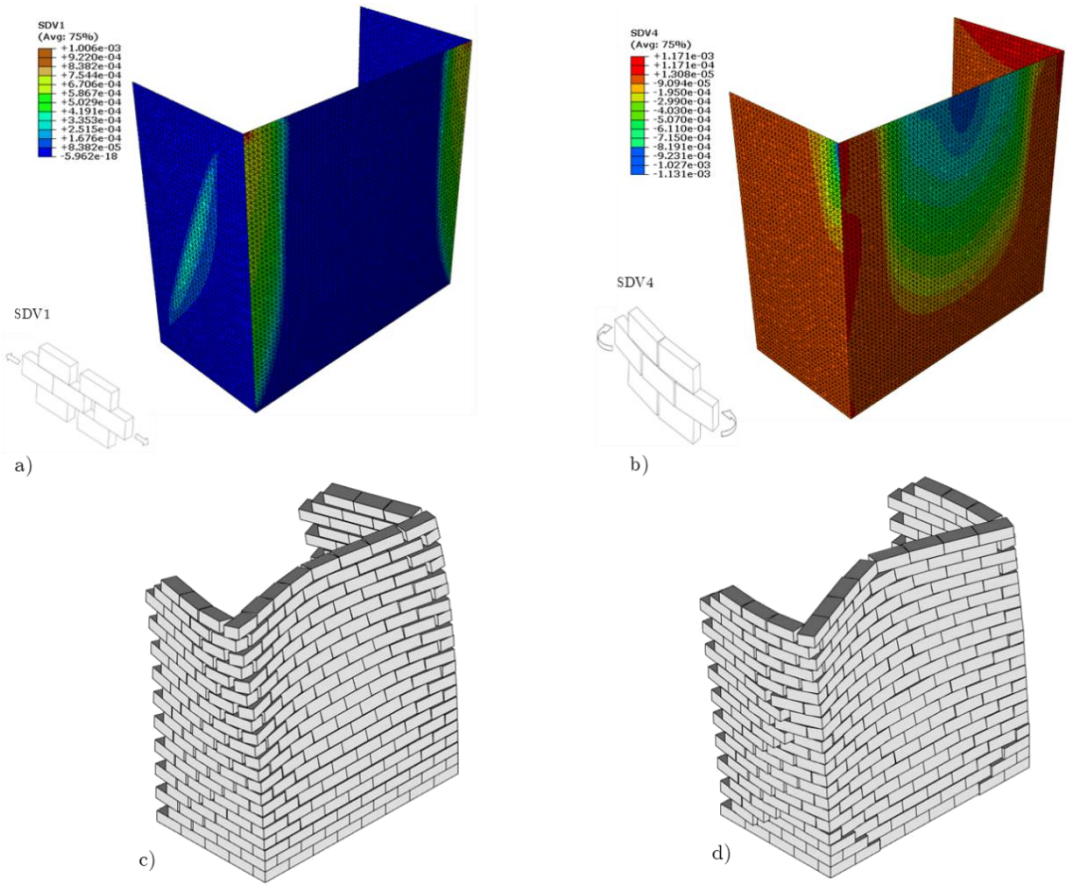

FIGURE 10. Test S5: sensitivity analyses to the friction coefficient ($\mu = 0.4$ in the Figure). a-b) Plastic strain distribution for FE model; c) associative and d) non-associative failure modes predicted with the RB model.

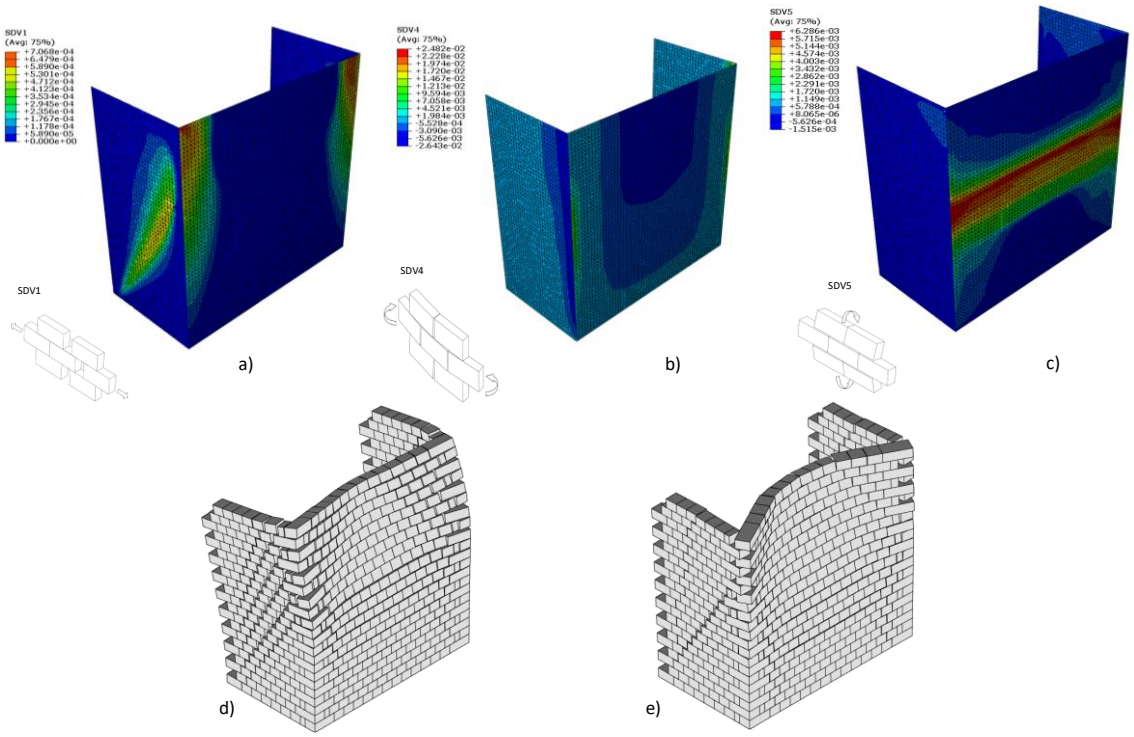

FIGURE 11. Test S5: sensitivity analyses to the size ratio (b=40 mm in the Figure). a)-c) Plastic strain distribution for FE model; d) associative and e) non-associative failure modes predicted with the RB model.

4.3. Sensitivity analysis to RBM starting conditions and FE mesh size

In the case of the rigid block model, a sensitivity analysis to starting conditions was carried out for the iterative solution procedure used to take into account non-associative sliding behaviour. The results show that the convergence behaviour is only slightly influenced by starting conditions when varying the initial value of the normal forces in the range considered (Fig. 12). In the case of specimen S22, it was observed that the number of iterations required to converge was less than that required for the standard iterative procedure using the associative solution as a starting point. However, in general CPU times were only slightly affected by the starting value of normal forces, also due to the limited number of blocks comprised in these case studies. Further discussion on this issue is presented in Section 6, where a large-scale model of a masonry church is analysed.

In Figure 13, the outcomes derived from the FE analyses are represented in terms of collapse load factor α_c versus the dimension of finite elements considered for the discretization. For each of the two prototypes, four different meshes were adopted, obtained reducing the dimension of the mesh elements as reported in Fig.13. As highlighted in the figure, some of the numerical solutions slightly exceed the RBM results. This should be related to the inherent effect of the discretization, which characterizes the FEM, leading to mesh-dependent solutions, that approach from above the RBM one as the number of elements increases [30].

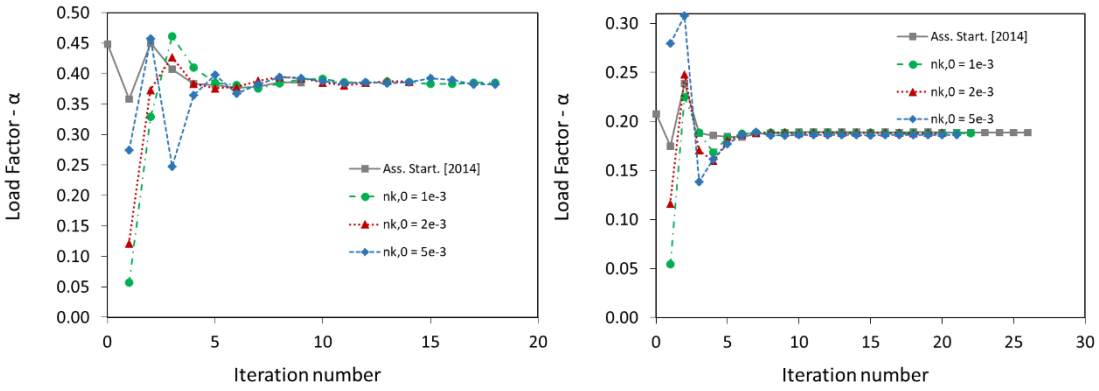

FIGURE 12. RBLA model: convergence plots and sensitivity analyses to starting conditions.

It is worth noting that the numerical solution converges to a value lower than the RBM one. This is not surprising as the FE model is based on the homogenization theory, where the characteristic size of the block (its height or width) has to be small enough when compared with the characteristic length of the problem, such as the wall's height or width [30].

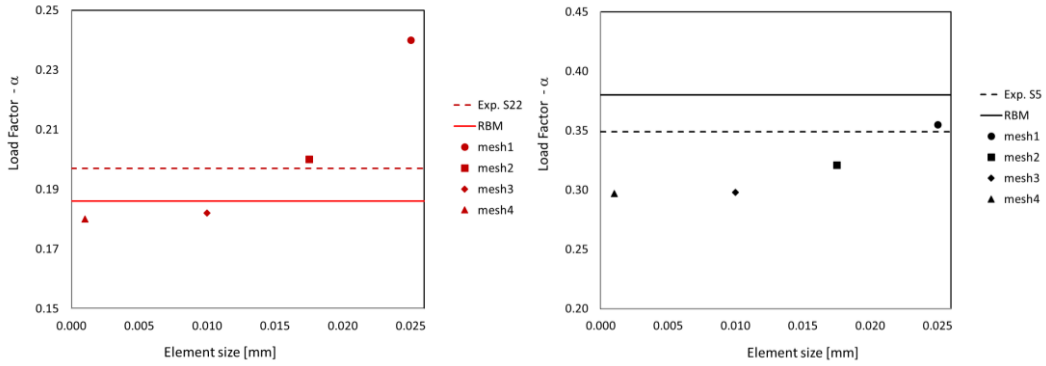

FIGURE 13. Sensitivity analyses to mesh size for FE model.

5. NUMERICAL CASE STUDY OF A MASONRY CHURCH

The numerical case study under investigation is a masonry construction representative of a typical ancient church characterized by a longitudinal plan, in the form of the Latin Cross. The case study was inspired by the church of San Nicolò di Capodimonte (Camogli, Genova, Italy), mainly for the dimensions of the different part of the buildings, the type of macro-elements (i.e. the façade, the triumphal arches, the nave, the transept, the apse and the bell tower) as well as for the texture of the limestone block masonry which was used in this case (Fig. 2a).

A long single nave, of about 18 meters, is crossed by a transept 14 meters large (Fig. 14). A chapel and a bell tower are located in the transept next to the apses. The bell tower is about 17.0 m height while the nave is 14.0 m height. The roof structure was not taken into account in the analysis because the focus of the present study was to compare the two modelling approaches on the basis of the response of vertical bearing structures only, rather than to perform a capacity

assessment of the real building. Moreover, it should be noted that possible rubble masonry sections - which could be reasonably used in thicker parts of the real case study - were treated as single leaf walls to restrict the number of configurations and geometric parameters affecting the response of the numerical models.

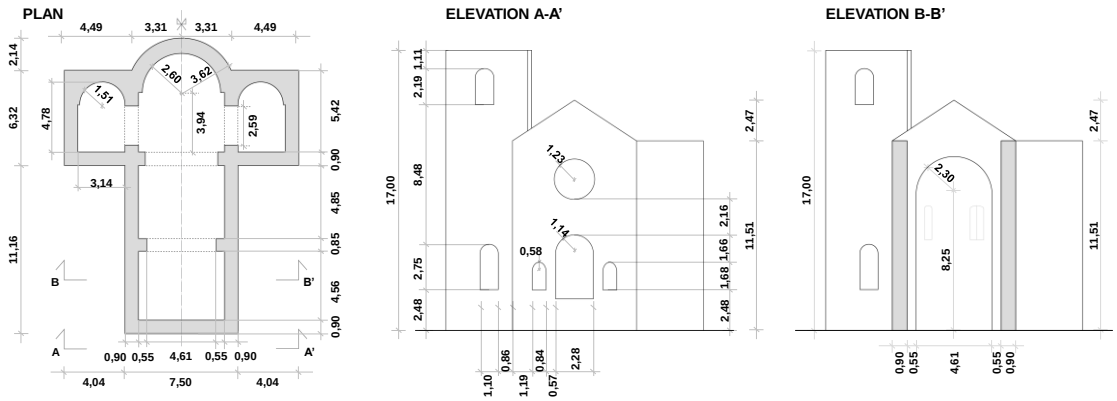

FIGURE 14. Dimensions of the numerical case study of an ancient masonry church building.

A rigid block model and a finite element model were generated to investigate the structural behaviour of the construction under lateral loads (Fig. 15).

The rigid block assemblage was generated in a computer aided design (CAD) environment first and then imported in an original software tool implemented in a MATLAB® graphical user interface (GUI) environment. The GUI allow to specify material properties, boundary and loading conditions and includes routines to solve the limit analysis problem underlying the collapse mechanism analysis as a second order cone programming problem [44].

The CAD model was generated in Autodesk AutoCAD® using blocks with attributes for each recurrent block type of the masonry assemblage. The Cartesian coordinates of the vertexes of each block type, the centroid and the coordinates of vertexes associated to each contact interface are modelled using object 'points' and position tags are applied to them. Additional attributes are included to store the block volume and the number of contact interface associated to each set of nodes.

The discrete rigid block model of the church is made of 5161 blocks and 49976 contacts (Fig. 15a). The average block size is 570 x 900 x 275 mm. The unit weight of masonry blocks for numerical simulation is 18.0 kN/m^3 and the friction coefficient at block interfaces is 0.6.

As in the case of small wall components, a distribution of lateral loads expressed as a factor of the self-weight was considered to simulate the effects induced by seismic actions. This distribution of lateral loads was set in accordance to code provisions comprising verification of local failure mechanisms, where a single multiplier (i.e. the load factor) is generally used to magnify lateral loads as a function of the corresponding vertical loads at different levels. However, it should be noted that alternative force distribution – such as those corresponding to

linearly varying accelerations – might be used, especially for the analysis of global failure mechanisms, which could strongly affect the estimation of the load factor associated to the onset of collapse behaviour.

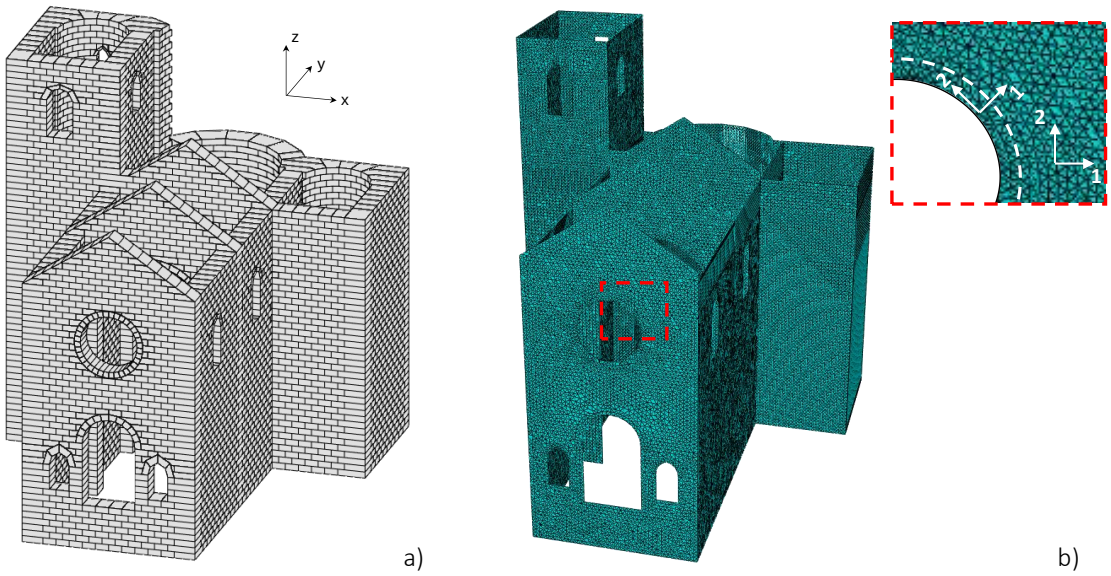

FIGURE 15. a) Rigid block model and b) Finite element model with detail of the bed joint orientations at the openings.

A 3D finite element model of the whole church was realized by using shell elements to model the middle plane of masonry walls [22]. The adopted mesh discretization, selected in accordance with the mesh sensitivity analyses discussed in Section 4, is made of 64993 shell elements for a total of 33300 nodes. Boundary conditions were applied restraining horizontal and vertical displacements for all the nodes at the ground level. The model was implemented in the FE code Abaqus and the non-linear behavior of the masonry was described by mean of the constitutive law summarized in the previous section. The FE model is also able to reproduce the bonding pattern above the openings varying the orientation of the bed joints as represented for the RB model (Fig. 15).

The height *a* and the width *b* of the blocks were set equal to 275 and 570 mm, respectively, while the friction coefficient and cohesion were posed equal to 0.6 and to 0.0, according to the parameters adopted in the rigid block model. The mechanical parameters needed for the definition of the elastic tensor **C** was assumed equal to the parameters in Table 1. First, the building was analyzed under constant vertical loads deriving from the own weight. The total weight of the church was around 18500 KN. After the application of the self-weight, a uniform distribution of lateral loads induced by seismic action was considered, where each finite element was subjected to horizontal loads proportional to the weight.

The rigid block and finite element numerical analyses were carried out on the same hardware in order to compare CPU times, that is using a 4.0 GHz Intel Core i7-6700k Processor with 32.0 GB of RAM.

6. RESULTS OF COLLAPSE MECHANISM ANALYSIS

Two different loading directions were considered for horizontal loads: the transverse direction (x-axis in Fig. 16a), parallel to the transept, and the longitudinal direction (y-axis in Fig 6b) parallel to the nave.

In Figs. 16a and 17a, the failure mechanism obtained with the rigid block model and the plastic strain field at failure for the finite element model are reported for the lateral loads acting along the x-axis. Both the models predict a collapse mechanism that essentially involves in-plane failures in the main facade and in the triumphal arches parallel to the main facade. The formation of diagonal cracks is observed in the façade between the openings, while the longitudinal walls parallel to y-z plane remain almost undamaged.

With respect to the second loading condition, Figs. 16b and 17b report the failure mechanism obtained for lateral loads along the y-axis and, in this case, both models predict the overturning of the main façade and of a portion of the sidewalls.

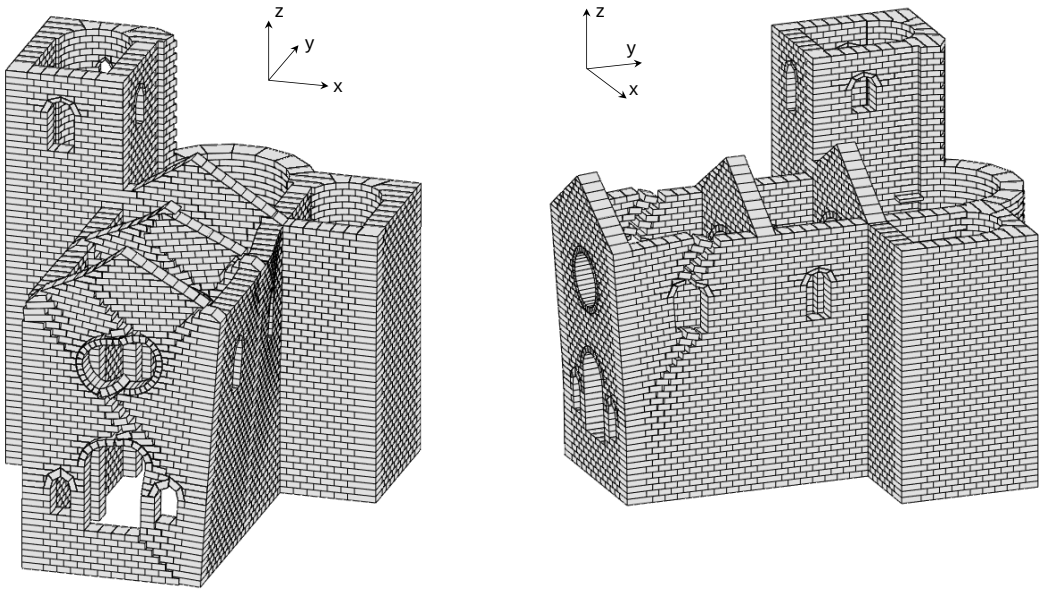

FIGURE 16. RB model of the church: non-associative failure modes for lateral load applied along the x-axis (a) and along y-axis (b).

The failure load multipliers, for the RB and the FE models, are summarized in Table 2. In the case of the rigid block model, both the associative and non-associative solutions are reported. It is worth noting that the results obtained from RB and FE models are in a good agreement, both

in terms of failure mode and in terms of collapse load multiplier, when the associative formulation of the RB model is considered. With reference to this last case, a discrepancy in the failure load multiplier of about 5.3% and 3.5%, between RB and FE models, is observed for lateral loads acting along x or y direction, respectively.

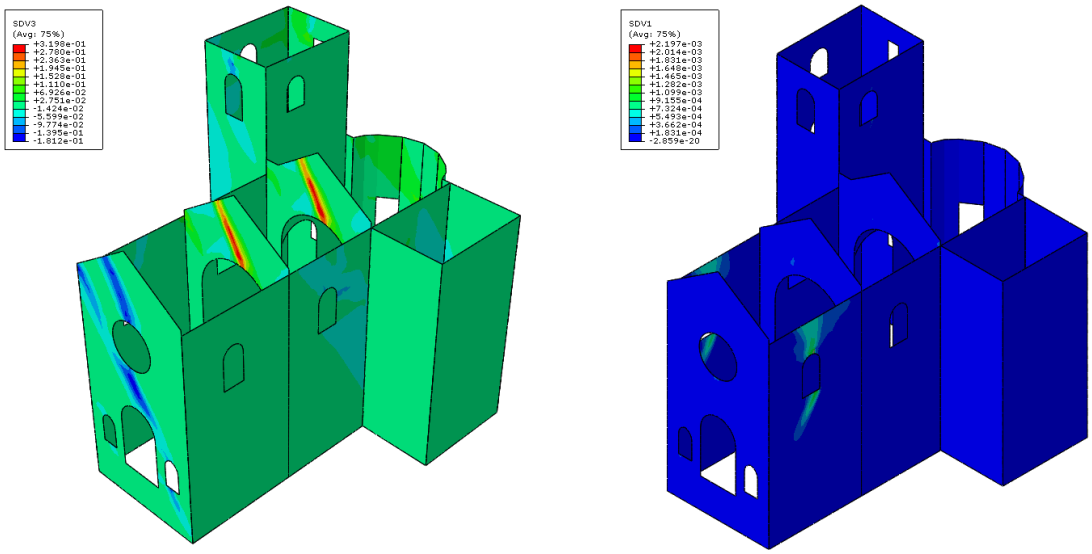

FIGURE 17. FE model of the church: plastic strain concentration at failure for lateral load applied along the x-axis (a) and along y-axis (b).

For the RB model, it is shown that the difference of associative and non-associative collapse load multipliers is up to 10 percent. It is also interesting to note that the associative solution is obtained in about 12 seconds, which is a reasonable CPU time considering the number of variables associated to the numerical model. As reported in Table 2, the average CPU time evaluated on the total number of load steps is about 25-27 seconds. Considering the high number of variables needed to define the model, the results can be considered reasonable.
In Fig. 18, the plot of the load multiplier versus the displacement at the control point, for the FE analyses, is represented, for both the directions, *x* and *y*, of the lateral loads. The control point was located in all the cases at the maximum displacement point, that was the same for the two lateral loads directions, that is the higher point of the façade. In the same Fig.8, are represented the results in terms of failure load multiplier of RB analyses, too.

Sensitivity analysis to the friction coefficient, in the case of lateral load applied along the x-axis and y-axis, was developed with both the models. For both the nonlinear models, different μ values generated only a change in the value of collapse load multiplier, without varying the collapse mechanism, always characterized the by in-plane failure of the main façade for loads acting along x-axis and by overturning of the façade in the case of horizontal loads along y-axis. Higher values of μ correspond to higher values of collapse load multipliers (Fig. 19a).

TABLE 2. Failure load multipliers and CPU time.

Lateral loads	μ	Rigid block model				Finite element model	
		Associative		Non-associative formulation		Associative	
		α_{assoc}	CPU Time (s)	$\alpha_{non\ assoc}$	CPU Time (s)	α_c	Average CPU Time (s)
x-axis	0.6	0.221	12.5	0.201	126.1	0.210	25.7
y-axis	0.6	0.237	12.3	0.224	118.9	0.229	26.2

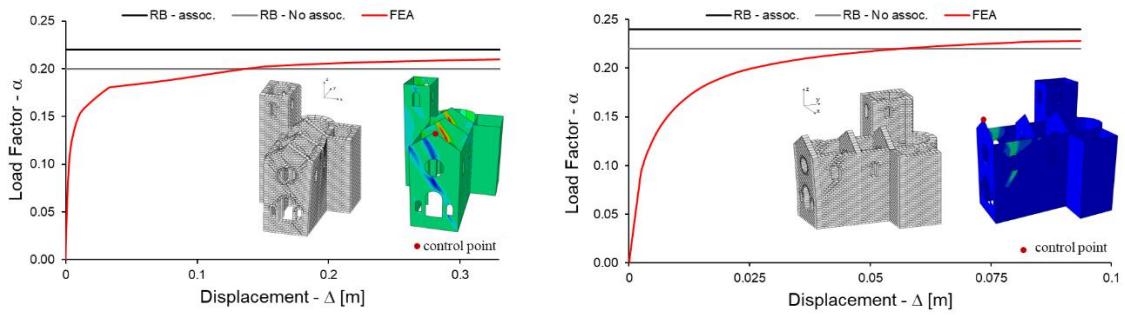

FIGURE 18. Comparison between RBLA and FEM results in terms of load factor vs displacement: a) x-axis; b) y-axis.

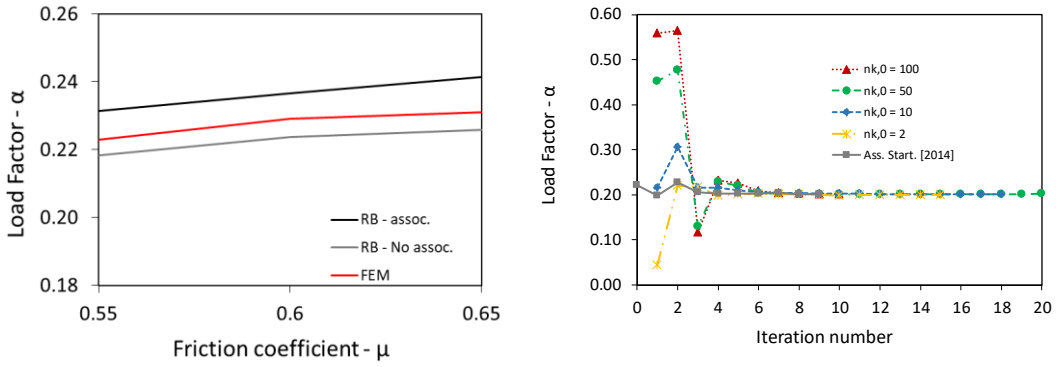

FIGURE 19. a) Sensitivity analysis to friction coefficient for lateral load applied along the y-axis; b) RBM convergence plot and sensitivity analysis to starting conditions.

In Figure 19b) the sensitivity to starting conditions is also shown for the rigid block model. Also in this case, the results show that the predicted value of the load factor is not affected by starting conditions. As for computational efficiency, in most cases the number of iterations required to converge is larger than that required for the associative starting solution procedure. Thus, the CPU time which is saved in the first iteration when a uniform force distribution is used for starting – rather than calculating the associative solution – is spent on the larger number of iterations required to converge.

Finally, in order to capture possible local failure mechanisms, nonlinear analyses considering lateral loads acting only to the bell tower along the x-axis, were carried out. The results of the analyses are reported in Fig.20, for the RB and the FE models.

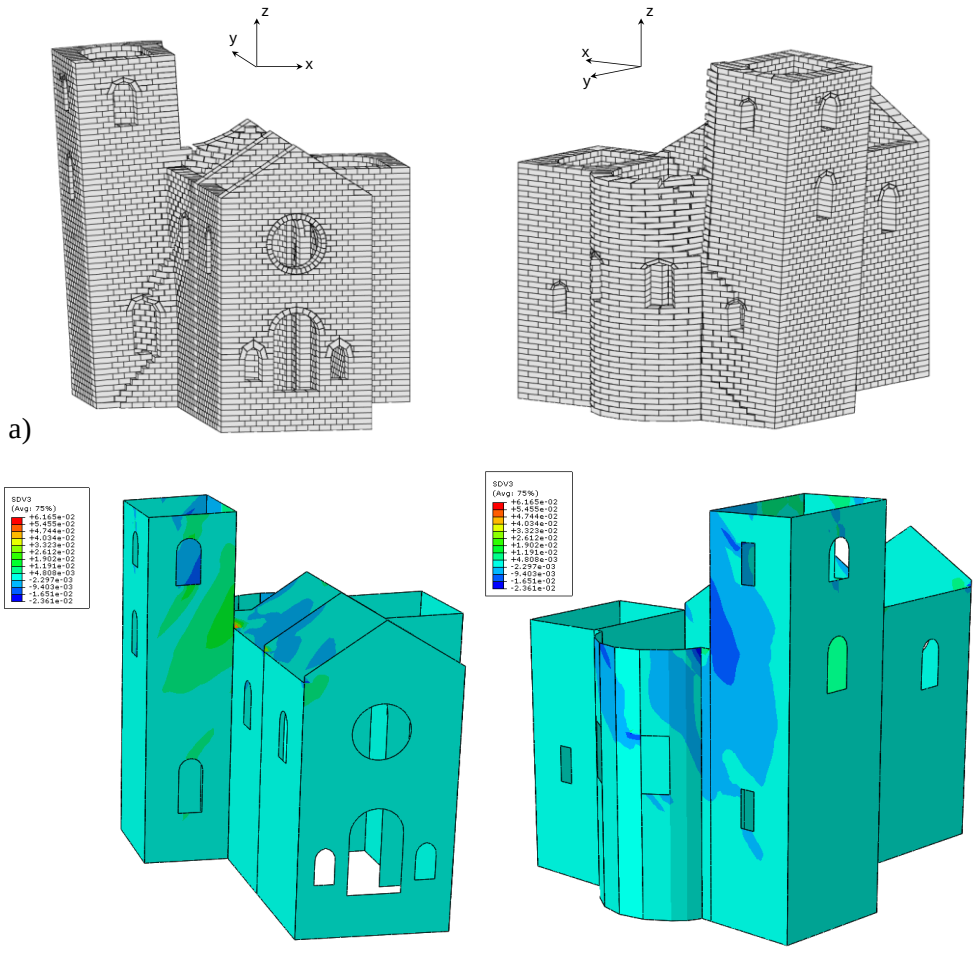

FIGURE 20. Lateral load applied only to the bell tower along the x-axis: a) non-associative failure mode for RB model ($\alpha_{non\text{-}assoc}$ = 0.339) and b) plastic strain concentration at failure for FE model (α_c = 0.345).

In this last case, while the two analyses returned failure load values rather similar between them, the results in terms of collapse mechanism, are not in perfect agreement: the RB model returns a failure mechanism involving the apse and the lower part of the bell tower, while for the FE model the collapse involves the apse but also the upper part of the bell tower.

Such a discrepancy in the failure mechanisms can be ascribed to the different bond pattern adopted in the two models to connect the bell tower. As a consequence, in the case of the rigid block model, the collapse mechanism also involves the triumphal arch with sliding and opening failures in the piers and at the top (Fig. 21), while for the FE model these failure mechanisms in the triumphal arch were not observed.

It is worth observing that, the failure load multiplier corresponding to this last analysis was higher than those deriving from the previous nonlinear analyses.

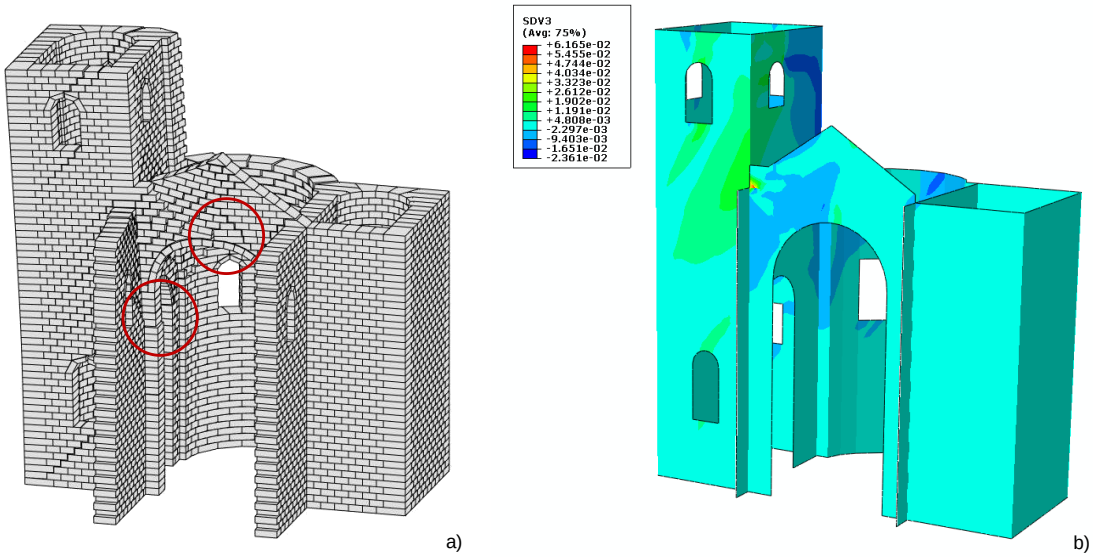

FIGURE 21. Lateral load applied only to the bell tower along the x-axis: Comparison of predicted associative failure mechanism at the triumphal arch between the nave and the transept.

In order to remark differences and similarities, the results from the two nonlinear models in terms of failure modes were overlapped in Fig. 22. Since the rigid block model provided very similar failure mechanisms for the associative and non-associative formulation, the overlapping of the results was carried out between the FE model and the associative formulation of the RB model. For the nonlinear analyses with lateral loads acting along *x* and *y* axes, a good correspondence between the plastic strain concentration derived from FE analyses and the opening of the joints from the RB model was observed. For the last case of lateral loads acting only on the bell tower, the discrepancy between the results, above described, is highlighted in Fig.22 c).

Finally, sensitivity analysis to block size were carried out also in this case to evaluate the effects on the predicted failure mechanism and corresponding load factors. The results obtained adopting blocks with the same height but splitting in half their base are shown in Figure 23 in the case of lateral loads acting along x-axis.

It is shown that the collapse modes are only slightly affected by the block size: as expected the crack pattern is now characterized by an almost vertical crack above and below the rose windows while in the previous case the crack exhibits a diagonal trend from the upper left corner up to the lower right corner of the façade. The reduction in the collapse load factors was equal to about 30.4 and 33.5 percent, for FE and RB model, respectively.

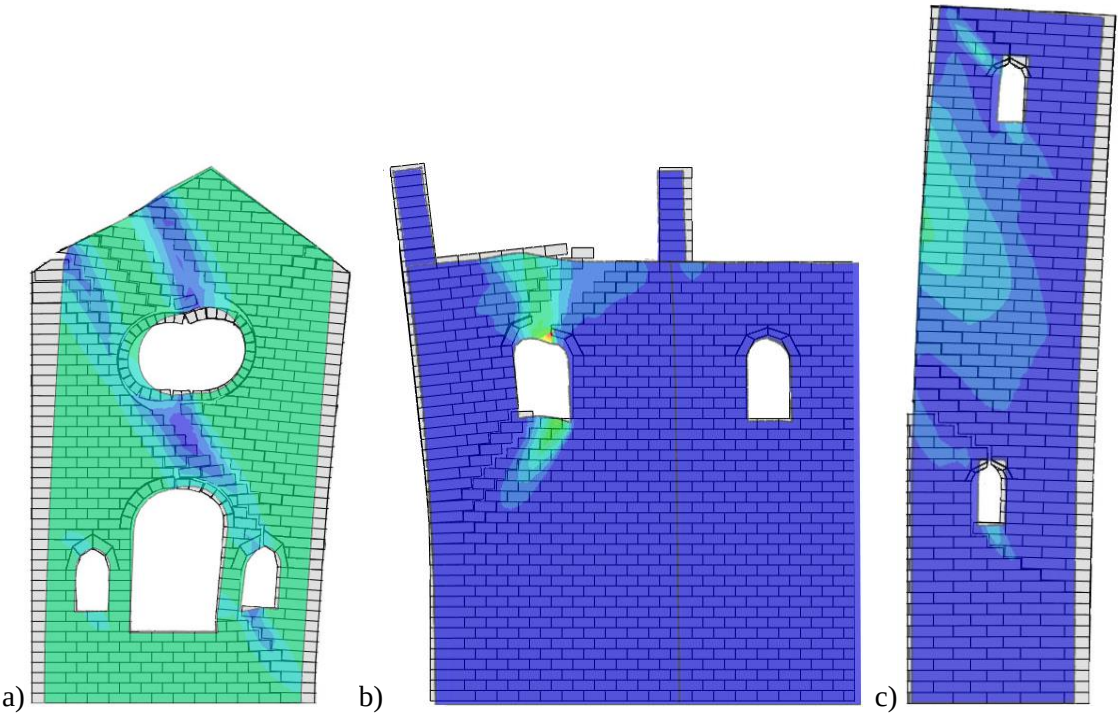

FIGURE 22. Overlapping of the associative failure modes: a) lateral load along x-axis; b) lateral load along y-axis; c) lateral load only acting on the bell tower.

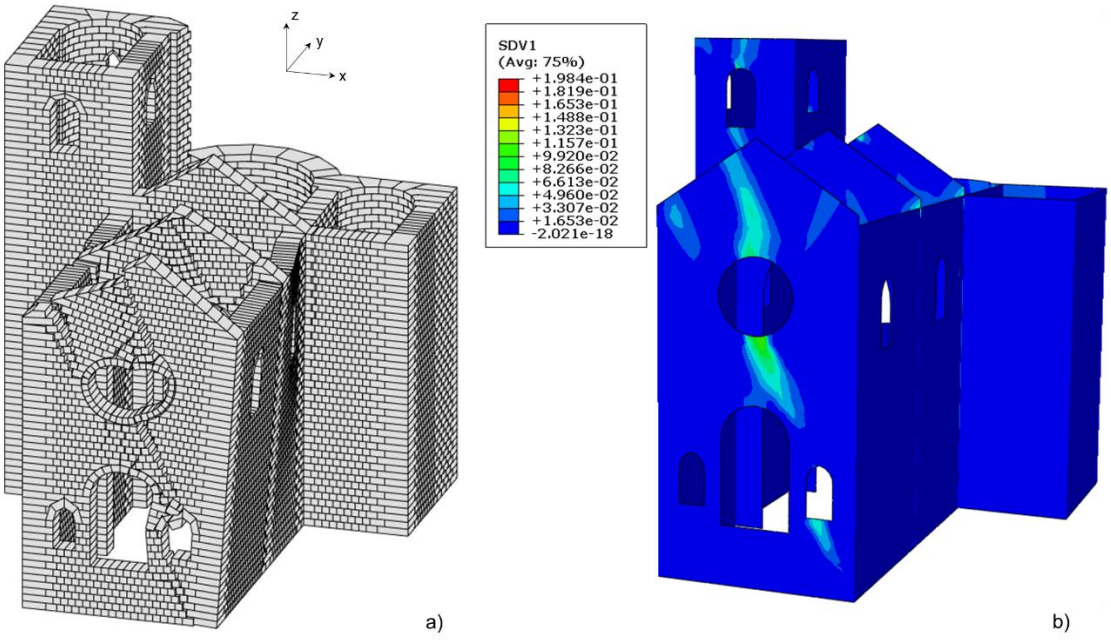

FIGURE 23. Lateral load applied along the x-axis. a) Non-associative RB failure mechanism ($\alpha_{non\text{-}assoc.}$ = 0.161) and b) plastic strain FE distribution at collapse predicted for the reduced block size (α_c = 0.167).

7. CONCLUSIONS

A discrete rigid block model and a continuous finite element model of small scale wall components and of an ancient masonry church building under lateral loads were generated in order to compare the outcomes of different modelling approaches when masonry is schematized as an assemblage of infinite resistant units interacting at Coulomb frictional interfaces.
The comparison between the numerical outcomes from the two models was carried out in terms of failure modes and deformed configurations, as well as in terms of lateral loads promoting the collapse when varying mechanical and algorithm parameters.

A good agreement of failure mechanisms was observed, indicating the ability of the discrete and the continuous models to capture similar local behavior and damages in the case of in-plane as well as in the case of out-of-plane collapse. Discrepancies in the predicted failure mechanism from the two models were observed only when the continuum model was not able to capture the masonry bond patterns considered in the rigid block model, as it was in the case of the church bell tower.

Also, the computed load factors were very similar in the case of in-plane failure mechanisms and in a good agreement with experimental outcomes, with differences up to about 5 percent. Conversely, in the case of small scale wall components, a remarkable difference was noted between the predicted load factors corresponding to out-of-plane failure mechanisms, which can be ascribed to the simple contact formulation adopted for the rigid block model.

As for computational efficiency, sensitivity analysis to starting conditions showed that CPU time is only slightly affected in the case of the rigid block model. Longer CPU time is needed to obtain a solution with FE analysis, considering that the continuum model requires a dense mesh to describe strong localization of plastic strains. Sensitivity analysis to mesh size also showed that the FE model underestimates the load factor predicted with the rigid block model, in accordance to the adopted homogenization theory.

An advantage of the adoption of the two models in predicting failure mechanisms typical of ancient masonry constructions lies in the few mechanical parameters required for calibration, namely the friction coefficient and masonry bond pattern. It should be noticed that more accurate models are available in the literature (e.g. implementing constitutive laws able to describe the nonlinear mechanical behavior of masonry). However, the use of such models generally requires many data input, which is often hardly available in practice. In this perspective, the nonlinear models presented in this study might represent a good compromise

among the reliability of results [22,30,32,34-36], the quality of input data, the accuracy of the analysis and the computational costs.

It is also worth noting that, in the case of the modelling approaches adopted in the present study, the collapse mechanisms are directly provided through the analysis and not a-priori defined, as it happens in the case of the analytical models for mechanism analysis suggested by different national guidelines [7-8, 37]. As such, the considered numerical approaches represent promising tools for the analysis of the most vulnerable mechanisms in historic masonry buildings under earthquakes.

However, since the two models were formulated for masonry walls with regular bond patterns, both the approaches are not able to capture local failure modes of multi-leaf or rubble masonry. Moreover, considering that the present study was focused on the response of vertical bearing structures, the modelling of curved and roof structures, such as masonry vaults and trusses, represent important issues for further development of the present study.

ACKNOWLEDGEMENTS

The financial support of Consortium 'ReLUIS-Italian Department of Civil Protection' (ReLUIS-DPC 2014-2018 and 2019-2021 Projects), Research Line Masonry structures is acknowledged.

REFERENCES

[1] D'Ayala, D., and E. Speranza. 2003. Definition of collapse mechanisms and seismic vulnerability of historic masonry buildings. Earthquake Spectra:19 (3):479–509. doi:10.1193/ 1.1599896.

[2] Lagomarsino, S. 2006. On the vulnerability assessment of monumental buildings. Bull Earthquake Eng.: 4:445–463 DOI: 10.1007/s10518-006-9025-y.

[3] Lagomarsino, S. 2015. Seismic assessment of rocking masonry structures. Bulletin of Earthquake Engineering, 13 (1), pp. 97-128.

[4] Sorrentino, L., D'Ayala, D., de Felice, G., Griffith, M.C., Lagomarsino, S., Magenes, G. 2017. Review of out-of-plane seismic assessment techniques applied to existing masonry buildings. *International Journal of Architectural Heritage*, 11 (1), pp. 2-21.

[5] Abrams, D.P., Al Shawa, O., Lourenço, P.B., Sorrentino, L. 2017. Out-of-plane seismic response of unreinforced masonry walls: Conceptual discussion, research needs, and modeling Issues. *International Journal of Architectural Heritage*, 11 (1), pp. 22-30.

[6] de Felice, G., and R. Giannini. 2001. Out-of-plane seismic resistance of masonry walls. Journal of Earthquake Engineering 5 (2):253–71. doi:10.1080/13632460109350394.

[7] Decreto del Ministero delle Infrastrutture e dei Trasporti 17 gennaio 2018. Aggiornamento delle norme tecniche per le costruzioni. Gazzetta Ufficiale della Repubblica Italiana n. 42, Supplemento Ordinario n. 8.

[8] Circolare del Ministero delle Infrastrutture e dei Trasporti 21 gennaio 2019, n. 7 C.S.LL.PP. Istruzioni per l'applicazione dell'«Aggiornamento delle "Norme tecniche per le costruzioni"» di cui al decreto ministeriale 17 gennaio 2018. Gazzetta Ufficiale della Repubblica Italiana n. 35, Supplemento ordinario n. 5.

[9] Roca, P., Cervera, M., Gariup, G., Pela', L. 2010. Structural Analysis of Masonry Historical Constructions. Classical and Advanced Approaches. Arch Comput Methods Eng:17:299-325.

[10] Reccia, E., Milani, G., Cecchi, A., Tralli, A. 2014. Full 3D homogenization approach to investigate the behavior of masonry arch bridges: The Venice trans-lagoon railway bridge. *Construction and Building Materials*; 66: 567-586.

[11] Smoljanović, H., Živaljić, N., Nikolić, Ž. and Munjiza, A. 2018. Numerical analysis of 3D dry-stone masonry structures by combined finite-discrete element method. *International Journal of Solids and Structures*, 136-137, 150-167, DOI:10.1016/j.ijsolstr.2017.12.012

[12] Baraldi, D., Reccia, E., and Cecchi A. 2018. In plane loaded masonry walls: DEM and FEM/DEM models. A critical review. *Meccanica*, 53 (7), 1613-1628, DOI: 10.1007/s11012-017-0704-3.

[13] Baraldi, D. and Cecchi, A. 2017. A full 3D rigid block model for the collapse behaviour of masonry walls. *European Journal of Mechanics, A/Solids*, 64, 11-28, DOI: 10.1016/j.euromechsol.2017.01.012

[14] Livesley, R.K. 1992. A computational model for the limit analysis of three-dimensional masonry structures. *Meccanica*; 27(3): 161-172.

[15] Gilbert, M., Melbourne, C. 1994. Rigid-block analysis of masonry structures. *Struct Eng*; 72(21): 356-61.

[16] Baggio C, Trovalusci P. Limit analysis for no-tension and frictional three dimensional discrete systems. Mech Struct Mach 1998;26:287–304.

[17] Baggio C, Trovalusci P. Collapse behaviour of three-dimensional brick block systems using non-linear programming. Struct Eng Mech 2000;10(2):181–95.

[18] Orduña, A., Lourenço, P.B. 2005. Three-dimensional limit analysis of rigid blocks assemblages. Part I: torsion failure on frictional joints and limit analysis formulation, *Int. J. Solids Struct.*; 42(18-19): 5140-5160.

[19] Portioli, F., Cascini, L., D'Aniello, M., Landolfo, R. A rigid block model with cracking units for limit analysis of masonry walls subject to in-plane loads (2012) Civil-Comp Proceedings, 99.

[20] K. Sab. Yield design of thin periodic plates by a homogenization technique and an application to masonry walls. C. R. Mecanique 2003;331(9):641646.

[21] Sab, K., Cecchi, A., Dallot, J. Determination of the Overall Yield Strength Domain of Out-of-Plane Loaded Brick Masonry. International Journal for Multiscale Computational Engineering 5(2):83-92, 2007.

[22] de Felice G. and Malena M. Crack pattern prediction in masonry. Journal of Mechanics of Materials and Structures. *Submitted for publication.*

[23] de Buhan P, de Felice G. A homogenization approach to the ultimate strength of brick masonry, J. Mech. Phys. Solids 1997;45(7):1085-1104.

[24] Angelillo M, Cardamone L, Fortunato A. A numerical model for masonry-like structures, Journal of Mechanics of Materials and Structures 2010;5(4):583-615.

[25] Caliò I, Marletta M, Pantò B. A new discrete element model for the evaluation of the seismic behaviour of unreinforced masonry buildings. Engineering Structures 2012;40:327-338.

[26] Anthoine A. Homogenization of periodic masonry: Plane stress, generalized plane strain or 3D modelling? Commun. Numer. Methods Eng. 1997;13(5):319–326.

[27] Zucchini A, Lourenço PB. A micro-mechanical model for the homogenisation of masonry. Int J Solids Struct 2002;39(12):3233–3255. http://dx.doi.org/10.1016/S0020-7683(02)00230-5.

[28] Milani G, Lourenço PB, Tralli A. Homogenised limit analysis of masonry walls, Part I: failure surfaces. Comput. Struct 2006;84(3):166–180.

[29] Sacco E. A nonlinear homogenization procedure for periodic masonry. European Journal of Mechanics, A/Solids 2009;28(2):209-222.

[30] de Felice G, Amorosi A, Malena M. Elasto-plastic analysis of block structures throught a homogeneization method. Int J Numer Analyt Methods Geomech 2010;34(3):221-247.

[31] Marfia S, Sacco E. Multiscale damage contact-friction model for periodic masonry walls. Computer Methods in Applied Mechanics and Engineering 2012; 205-208(1):189-203.

[32] Portioli, F., Casapulla, C., Gilbert, M., Cascini, L. 2014. Limit analysis of 3D masonry block structures with non-associative frictional joints using cone programming. *Computers and Structures*; 143: 108-121.

[33] Portioli, F., Casapulla, C., Cascini, L., D'Aniello, M., Landolfo, R. Limit analysis by linear programming of 3D masonry structures with associative friction laws and torsion interaction effects (2013) Archive of Applied Mechanics, 83 (10), pp. 1415-1438.

[34] Amorosi A, Boldini D, De Felice G, Malena M. Tunnelling-induced deformation on a masonry structure: a numerical approach. In: Geotechnical aspects of underground construction in soft ground. Proceedings of the 7th international symposium on geotechnical aspects of underground construction in soft ground 2012;353–359.

[35] Amorosi A, Boldini D, de Felice G, Malena M, Sebastianelli M. Tunnelling-induced deformation and damage on historical masonry structures. Géotechnique 2014;64(2):118-130.

[36] Amorosi A, Boldini D, de Felice G, Lasciarrea WG, Malena M (2016). An integrated approach for geotechnical and structural analysis of the Nynphaeum of Genazzano. Structural Analysis of Historical Constructions: Anamnesis, diagnosis, therapy, controls - Proceedings of the 10th International Conference on Structural Analysis of Historical Constructions SAHC 2016;503-510.

[37] Italian Guidelines for the evaluation and reduction of the seismic risk of cultural heritage, with reference to the Italian norm of constructions (DPCM 9/2/2011).

[38] Mistler M., Anthoine A., Butenweg C. In-plane and out-of-plane homogenisation of masonry, Comput. Struct. 85 (2007) 13211330.

[39] Koiter W.T. 1960. General theorems for elastic-plastic solids. Progress in solids mechanics, ed I. N. Sneddon and R Hill, 165(221), North-Holland, Amsterdam.

[40] Godio M, Stefanou I, Sab K. Effects of the dilatancy of joints and of the size of the building blocks on the mechanical behavior of masonry structures. Meccanica 2018;53(7):1629-1643.

[41] D. Goldfard, A. Idnani, "A numerical stable dual method for solving strictly convex quadratic programs". Mathematical Programming, 27, 1-33, 1983.

[42] M. Malena, R. Casciaro, "Finite element shakedown analysis of reinforced concrete 3D frames". Computers and Structures, 86, 1176-1188, 2008.

[43] Gilbert, M., Casapulla, C., Ahmed, H.M. 2006. Limit analysis of masonry block structures with non-associative frictional joints using linear programming. Computers and Structures, 84 (13-14), pp. 873-887.

[44] Cascini, L., Gagliardo, R., Portioli, F. LiABlock_3D: A Software Tool for Collapse Mechanism Analysis of Historic Masonry Structures (2018) International Journal of Architectural Heritage, Article in Press.

[45] Restrepo Vélez, L.F., Magenes, G., Griffith, M.C. Dry stone masonry walls in bending-Part I: Static tests (2014) International Journal of Architectural Heritage, 8 (1), pp. 1-28.

[46] Tran-Cao, T. 2009. Collapse analysis of block structures in frictional contact. PhD Thesis. School of civil and environmental engineering. Sydney (Australia): The University of New South Wales.

[47] Casapulla, C., Maione, A. Modelling the dry-contact interface of rigid blocks under torsion and combined loadings: Concavity vs. convexity formulation (2018) International Journal of Non-Linear Mechanics, 99, pp. 86-96.